

Corrosion performance of mild steel and epoxy coated rebar in concrete under simulated harsh environment

Corrosion performance of mild steel

657

Muazzam Ghous Sohail, Mohammad Salih and Nasser Al Nuaimi
Center for Advanced Materials, Qatar University, Doha, Qatar, and

Ramazan Kahraman

*Department of Chemical Engineering, College of Engineering,
Qatar University, Doha, Qatar*

Received 4 December 2018

Revised 26 February 2019

23 March 2019

Accepted 23 March 2019

Abstract

Purpose – The purpose of this paper is to present the results of a two-year long study carried out in order to evaluate the corrosion performance of mild steel bare bars (BB) and epoxy-coated rebar (ECR) in concrete under a simulated harsh environment of chlorides.

Design/methodology/approach – The blocks are subjected to Southern Exposure testing. The electrochemical impedance spectroscopy (EIS), linear polarization resistance (LPR) and Tafel plot are performed to measure the polarization resistance and corrosion current densities of these rebars. Knife-peel test was performed to assess the adhesion between epoxy and underlying steel after two years of exposure.

Findings – Mild steel BB showed a high corrosion current density of $1.24 \mu\text{A}/\text{cm}^2$ in Tafel plots and a very low polarization resistance of $4.5 \text{ k}\Omega \text{ cm}^2$ in LPR technique, whereas very high charge transfer resistance of 1672 and $1675 \text{ k}\Omega \text{ cm}^2$ is observed on ECR and ECR with controlled damage (ECRCD), through EIS technique, respectively. EIS is observed to be a suitable tool to detect the defects in epoxy coatings. After two years of immersion in 3.89 percent NaCl solution, the mild steel BB were severely corroded and a considerable weight loss was observed, whereas under heavy chloride attack, ECR showed no deterioration of epoxy coating and neither any corrosion of underlying steel. Results of this study show that the durability of reinforced concrete (RC) structures with respect to corrosion could be enhanced by using ECR, especially in harsh climatic conditions.

Originality/value – The corrosion performance of mild steel and ECR in concrete under a simulating splash zone environment is evaluated. EIS was used to evaluate the health of epoxy and corrosion state of underneath steel rebars. EIS was able to detect the defects in epoxy. The durability of RC structures could be enhanced in harsh climate regions by using ECR.

Keywords Accelerated aging conditions, Corrosion in reinforced concrete, Epoxy-coated rebar, Infrastructure durability in harsh climate

Paper type Research paper

Nomenclature

Abbreviations and Symbols	Description	EIS	Electrochemical impedance spectroscopy
BB	Mild steel bare bars	HCP	Half-cell potential
CE	Counter electrode	LPR	Linear polarization resistance
ECR	Epoxy-coated rebar		
ECRCD	Epoxy-coated rebar with controlled damage	RC	Reinforced concrete
		RH	Relative humidity

The funding for this research was provided by the National Priorities Research Program of the Qatar National Research Fund (a member of Qatar Foundation) under the award no. NPRP 7-410-2-169. Authors would also like to thank Qatar Metals Coating Company (Q-Coat), Qatar Steel for providing the materials and support. The statements made herein are solely the responsibility of the authors and do not necessarily reflect the opinions of the Sponsor.



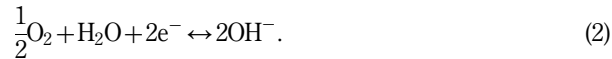
WE	Working electrode	I_{corr}	Corrosion current (μA)
SCE	Saturated Calomel Electrode	I	Electrical current (amp)
OCP	Open circuit potential	K	Constant in corrosion rate equation
A	Area (cm^2)		
a	Distance between the electrodes (cm)	ρ	Concrete resistivity ($\Omega.cm$)
		R_c	Concrete resistance (Ω)
B	Stern–Geary constant	R_{ct}	Charge transfer resistance ($k\Omega cm^2$)
β_a	Anodic Tafel slope constant (mV/dec)	R_p	Polarization resistance ($k\Omega cm^2$)
β_c	Cathodic Tafel slope constant (mV/dec)	R_2/R_{EP}	Rust layer/epoxy resistance (Ω)
C_2/C_p	Double layer capacitance ($\mu F.cm^{-2}$)	T	Exposure time (hrs)
D	Density (g/cm^3)	W	Mass loss (g)
E_{corr}	Corrosion potential (E_{corr})	V	Potential difference(Volt)
$E.W$	Equivalent weight (g/mol)		

1. Introduction

Reinforced concrete (RC) is the most used construction material for infrastructures, such as harbors, bridges, multistory buildings and industrial silos. The availability of raw materials, low cost and adaptability make concrete the most suitable selection, whereas mild steel is most commonly used as a concrete reinforcement, as both have a similar coefficient of thermal expansion. Concrete protects the steel rebar from corrosion for long periods of time due to its alkaline environment. However, in last few decades, the deterioration of RC structures due to the rebar corrosion has become a major challenge to the construction industry and a financial burden on the economy around the world (Dunn *et al.*, 2010). This problem is aggravated in the environments with higher temperature, relative humidity (RH), higher chlorides and CO_2 concentration (Al-Khaiat *et al.*, 2007; Al-Samarai, 2015; Pakkala *et al.*, 2019). The Arabian Gulf region is one such example where temperature frequently crosses $50^\circ C$ and RH 80 percent with a higher chloride concentration in air. Such extreme environmental conditions cause rapid and severe corrosion of the steel reinforcement and instigate the deterioration of RC structures well before the designed service life (Sohail *et al.*, 2018).

Deterioration process in RC structures consists of two distinct time phases: initiation and propagation (Tuutti, 1982). During the initiation phase, the aggressive agents (chloride ions or the carbonation front) penetrate the concrete cover and accumulate at the steel–concrete interface. No corrosion (deterioration) occurs in this phase, which usually lasts for several years (15–20) in normal quality concrete (Yingshu *et al.*, 2007). A passive oxide layer is formed at the steel surface due to the high concrete alkalinity, which prevents steel from corrosion. The propagation phase starts when a certain level of chloride ion concentration (threshold) reaches the steel–concrete interface or when concrete cover is carbonated, which lowers the pH of pore solution; as a result of these two phenomena, the passive layer becomes unstable and it is destroyed, initiating the corrosion process (Poon and Baldwin, 1990; Angst *et al.*, 2012; Sohail *et al.*, 2015; Tasker, 1985). The service lifespan of RC structures shortens once corrosion is initiated. The corrosion is a natural phenomenon in which steel tends to revert back to oxide form on the availability of suitable environments (i.e. presence of oxygen (O_2) and humidity (H_2O)). Corrosion process follows electrochemical laws wherein two half-cell reactions occur simultaneously at steel surface, as shown in Figure 1, the iron oxidation at anode sites

(Equation (1)), and the oxygen reduction at cathode sites, which consumes the free electrons from the anodic reaction, (Equation (2)) (Elsener *et al.*, 2003; Andrade and Alonso, 2004; Ahmad, 2009; Sohail, 2013; Poon and Baldwin, 1990):



The iron ions (Fe^{2+}) react with the hydroxide ions (OH^{-}) and form several phases of rust at the steel–concrete interface. The expansion of these rust products distresses the concrete around steel rebar as their volume is six times higher than the steel itself (Bazant, 1983; Liu and Weyers, 1998; Nasser, 2010; Duffó *et al.*, 2012). This induces the cracking and spalling of the concrete cover. The reduction in cross-sectional area of rebar due to corrosion either makes the RC structures unsafe to be in service or in some cases instigates the structural failure (Broomfield, 2007).

The salt spraying on highways to melt the snow caused corrosion problems in the bridges in North America and other countries with cold climate. To overcome this problem, a research was initiated by the National Institute of Standards in the USA, in the early 1970s, which resulted in epoxy-coated reinforcing bars (Manning, 1996; Keßler *et al.*, 2016). The optimum thickness required for corrosion protection, bond strength, and creep requirement was established to be 0.18 ± 0.05 millimeter (mm) (Manning, 1996). Around 60,000 highway bridges were built using ECR from the 1970s until 2004 in the USA (McDonald, 2009). Several reports and research papers have been published on the laboratory and field performance of ECR. Pyc (1998) performed a field study on 18 different bridges reinforced with ECR, having age between 7 and 20 years, in Virginia, US. It was concluded that epoxy loses its adhesion with steel surface over time, this was attributed to the moisture ingress rather than chloride attack. This adhesion loss caused the corrosion of the underlying steel. The enhancement of service life with ECR was not significant, especially once there was disbonding of epoxy layer.

However, Keßler *et al.* (2016) suggested otherwise, after evaluating the parapet of a 24-year-old ECR-reinforced concrete bridge in Switzerland. The bridge was a Swiss pilot project to test the effect of ECR on the durability of RC structures. After 24 years of service life in the area with XD3 exposure conditions, according to EN 206-1 (2000) (i.e. exposure with an average 10 days rain per month), it was observed that the epoxy was in good conditions with a shining green color; neither damage nor disbondment was noticed. Chloride contents were 0.7 percent by weight of concrete at the outer surface of the parapet and 0.05 percent at the steel–concrete interface, which is less than the chloride

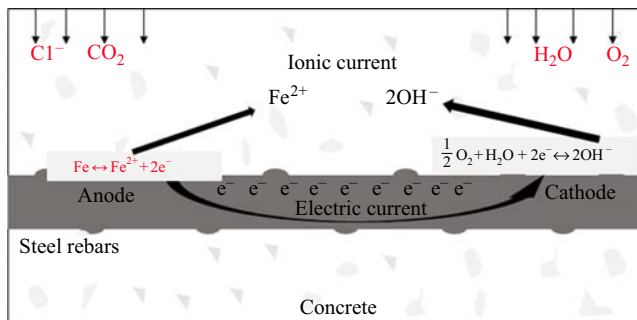


Figure 1. Corrosion process in reinforced concrete, showing anodes and cathode sites

threshold to initiate the corrosion at mild steel reinforcing bars. However, the moisture had not caused any disbondment, as observed by Pyc (1998). Further, the ECRs with controlled damaged were also used in some parts of the bridge's parapet. The pre-defined defects on the ECRs form macro-cells with uncoated rebar if there is an electrical connection. This causes the cathodic disbondment of epoxy at defects (Keßler *et al.*, 2016). Most of the bridges built in the USA had only the upper reinforcement layer of ECR and the bottom layer was of uncoated bare bars (BB). This could form macro-cells between a damaged portion of ECR, which act as a cathode, and an uncoated rebar, which will act as an anode. This might have caused the cathodic disbondment of epoxy, as observed by Pyc (1998).

Erdoğdu *et al.* (2001) tested the ECR in comparison with mild steel BB under seawater and synthetic 3 percent NaCl⁻ solution. The ECRs were used as received, and with 1 and 2 percent controlled damage. It was observed that after two years of exposure under the chloride environment, the undamaged ECR showed no signs of corrosion. The ECR with 1 and 2 percent damage showed very low corrosion current at the damaged area. Epoxy was difficult to be removed in the knife-peel test. Although the outcomes of studies are mixed, it has been established to date that the durability of civil infrastructure could be enhanced in conditions in which the corrosion problem is imminent (Khaled *et al.*, 1998; Pyc, 1998; Keßler *et al.*, 2016).

The Arabian Gulf is the most severely affected area due to the harsh climatic conditions. The Gulf seawater has the highest salinity of 38.9 g/l, groundwater chloride contents are up to 43 g/l (Qatalum, 2006). The researchers have proposed several techniques to enhance the durability of infrastructure under such environments. Maslehuiddin and Al-Amoudi (2007) studied the effectiveness of three possible methods, i.e., addition of supplementary cementing materials in concrete, use of coated rebar and concrete surface coating. It was observed that the use of coated rebar is the most feasible and effective way to overcome the durability issue of RC structures. Furthermore, since concrete cracking is unavoidable, and once the crack width reaches 80 micrometers (μm), the concrete diffusivity becomes equal to that of an open solution (Djerbi *et al.*, 2008). This further facilitates the chloride ingress. This is why the initiation phase could be prolonged by using high-performance concrete or larger concrete cover; however, the risk of corrosion initiation due to chloride cannot be completely eliminated. Hence, to prevent the corrosion initiation, use of corrosion-resistant steel, such as epoxy-coated rebar (ECR), is imperative. The epoxy provides a physical barrier against chloride ions to reach underlying steel. It also exhibits higher resistance to electric charge; hence, no macro-cells are formed in a reinforcement mesh. Since the expansive corrosion products are not formed at the steel-concrete interface to distress the concrete cover, spalling and cracking of concrete are avoided. To build a sustainable infrastructure, there is a dire need to adopt resilient construction materials that could minimize the damage caused by these aggressive environmental conditions suffered in the Arabian Gulf and other similar regions.

In this study, the comparison of corrosion damage caused by chloride environment to mild steel bare bar and ECR is established. The aim of the study was to evaluate whether the durability of RC subjected to the harsh environment of tidal zones could be enhanced by using ECR. Similar studies have been carried out by Rasheeduzzafar *et al.* (1992) and Erdoğdu *et al.* (2001). However, Rasheeduzzafar *et al.* (1992) used the chloride-bearing concrete instead of placing concrete samples in seawater. Erdoğdu *et al.* (2001) have evaluated the corrosion on ECR by half-cell potential and LPR techniques. The LPR technique applies direct current to polarize the steel rebar, which will not be able to pass through the epoxy, and hence would not yield accurate results. In this study, the corrosion behavior of ECR and mild steel BB is evaluated by electrochemical impedance spectroscopy (EIS), which applies AC polarization impulse. EIS is proven to be the most

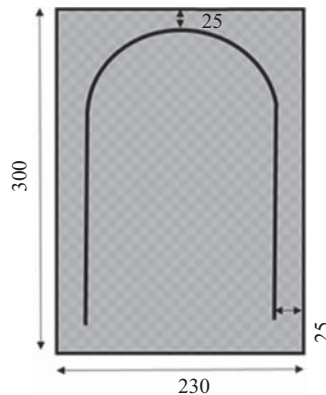
suitable tool to study the corrosion performance of epoxy coating and corrosion of the underlying steel. Results showed that the EIS technique could detect the damaged epoxy region of ECR. The employed accelerated aging technique could be a useful tool to test the durability behavior of innovative, corrosion-resistant steel bars (e.g. high chromium steel, stainless steel, galvanized steel and other high strength steels) in a short period of time. The results of this study will assist the engineers and designers in employing ECR as concrete reinforcement in harsh climatic zones, as encountered in Arabian Gulf.

2. Experimental details

2.1 Materials and Sample geometry

To evaluate the corrosion behavior, 16 mm diameter U-shaped mild steel BB, ECR or ECRCD were, respectively, embedded at the middle of concrete block samples of 230 mm × 300 mm × 70 mm dimensions. Figure 2 schematically presents the sample geometry. The U-shaped bent was provided to observe the effect of stress-induced corrosion on BB and the disbondment of epoxy and its effects on ECR corrosion. The ECRs were used in two conditions, as received (ECR) and with 3 mm diameter circular damage in epoxy at three locations (ECRCD). Three concrete block samples for each type of reinforcement were cast and designated as: BB-1, BB-2, BB-3, ECR-1, ECR-2, ECR-3, or ECRCD-1, ECRCD-2, ECRCD-3, respectively.

The chemical composition of steel rebar (mild steel BB, ECR and ECRCD) was the same as presented in Table I. The powder-based fusion-bonded (Bisphenol A, 2-Methylimidazole) epoxy was used for ECR and ECRCD. The average coating thickness was 11.5 and 12.5 mils



Note: All dimensions are in mm

Figure 2.
Schematic of concrete
block samples with
U-shaped
reinforcement steel
bars at the middle

%C	%Mn	%Si	%P	%S	%V	%Cu	%Ni	%Cr
0.27	0.72	0.15	0.01	0.02	0.01	0	0.02	0.02

Table I.
Chemical composition
of mild steel BB, ECR
and ECRCD

(292 to 317 μm) at top and bottom, respectively, which conforms to ASTM A775/A775M – 17 (2017) standards. A C40 concrete (40 MPa compressive strength) was selected to cast the samples. The mixture proportion of concrete is given in Table II. The ordinary Portland cement (OPC) type II (CEM-II), gabbro coarse aggregates, washed sand and polycarboxylate ether-based (PCE-202) superplasticizers were used for the concrete casting.

662

2.2 Accelerated aging conditions

Concrete samples were cured by immersion under water for 28 days. Then the southern exposure conditions (Virmani *et al.*, 1983; Funahashi, 1990) were applied by placing the samples in a salt spray chamber filled with 3.89 percent NaCl^- solutions (i.e. Arabian Gulf seawater) (Plate 1). Cycles of four days of ponding at 16–27°C, followed by three days of heating and drying at a target temperature of 52°C, were applied. This was to simulate the severe corrosive environments, especially encountered in marine tidal zones. These cycles continued for twelve weeks, then the continuous ponding under seawater at a target temperature of 32°C, for the following 12 weeks, was applied. This 24-week cycle was repeated 4 times for a total exposure time of 96 weeks. With wetting and

Table II.
Concrete
mixture proportion

Constituents	kg/m ³
Cement SRC	380
Sand	736
Aggregate 10 mm	590
Aggregate 20 mm	576
Water	178
Admixture	3.5
Total dry weight	2,463.5



Plate 1.
Concrete block
samples under Gulf
seawater inside a salt
spray chamber

drying cycles, the chloride ingress in concrete is ensured. Water carrying chlorides penetrates into the pores ions during ponding and evaporates during the drying cycle, leaving chloride ions at the concrete surface. The concentration gradient of chlorides increases at the concrete surface and diffusion process then transports these ions to the steel–concrete interface.

2.3 Test performed

Several electrochemical tests were carried out to evaluate the corrosion behavior of mild steel BB and ECR in the concrete immersed in seawater with 3.89 percent NaCl^- . Experimental plan was comprised of concrete resistivity, chloride profile, half-cell potential measurements, EIS, LPR, Tafel plots, gravimetric weight loss and knife-peel test. Following is the description of performed tests.

2.3.1 Concrete resistivity. The resistivity is a measure of concrete quality and an indicator of the corrosion risk (Polder and Hug, 2000). The lower the concrete resistivity, the higher will be the risk of corrosion, as the flow of ions (Fe^{2+} , OH^-) would be easier through concrete pores (Nagi and Whiting, 2004). The concrete surface resistivity was measured using Giatec® resistivity meter, which is based on four-point Wenner probe, thereby conforming with AASHTO TP 95 (2011). Figure 3(a) schematically presents the concept of measurement, whereas Figure 3(b) shows the measurements on concrete blocks. The bulk concrete resistance is measured in Ohms by injecting electrical current (I) through external electrodes and potential difference (V) is observed by central two electrodes (Figure 3). Resistivity of concrete was then obtained by Equation (3):

$$\rho = 2a\pi V/I, \quad (3)$$

where ρ is the concrete resistivity in Ohms.cm, and a is the distance in cm between the electrodes.

2.3.2 Chloride profiles. The chloride contents in concrete blocks at different depths, starting from top surface till the steel–concrete interface (i.e. 25 mm), were measured after an exposure of 2 years. The BS 1881: Part-124 (1998) standards were followed to obtain these chloride profiles. The concrete powder from selected depths was ground to pass through a sieve size of $125 \mu\text{m}$. This standard test is comprised of a wet chemical titration and the results are obtained in the % chloride ions contents by weight of concrete samples. However, most of the literature mentions chloride ion threshold values for corrosion initiation of mild steel reinforcement by % weight of cement. For this reason, the chloride contents are presented in % weight of cement too, whose quantity is known from concrete mix proportion.

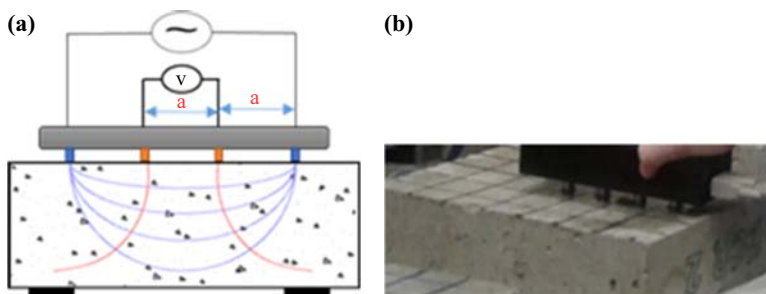


Figure 3.
(a) Schematic of resistivity measurements concept; (b) resistivity measurements on concrete blocks by Giatec® meter

2.3.3 Half-cell potential. The half-cell potential (HCP) values distinguish the active and passive corrosion zones on a concrete reinforcing steel bar. It is measured against a reference electrode (RE) according to ASTM C876-09 (2015). The Giatec® HCP measuring equipment, which uses copper/copper-sulfate (Cu/CuSO₄) (CSE) as an RE, was used in this study. Concrete blocks were marked by grids of 4 cm × 4 cm to get HCP contour mapping (Plate 2). The concrete block samples BB-1, BB-2 and BB-3 were drilled till rebar established an electrical connection (Plate 2). In case of ECR and ECRCD, the HCP measurements are not possible until the epoxy is removed and a direct connection to underlying steel is established; hence, concrete was removed from one corner to expose the rebar and then the epoxy was peeled off from a small portion. A concrete block sample for each type of reinforcement (BB-1, ECR-1 and ECRCD-1) was broken after HCP measurements for visualizing the corrosion state and epoxy condition.

2.3.4 Linear Polarization Resistance. HCP is a well established and most commonly used test to predict the rebar corrosion; however, it provides no information on corrosion kinetics. LPR, EIS and Tafel polarization techniques were employed to measure the corrosion current (I_{corr}) on the steel surface. A three-electrode setup, as shown in Figure 4, was used to obtain the curves for LPR, EIS and Tafel plots using Gamry® Potentiostat. The setup consisted of a working electrode (WE), which was reinforcing steel bar, a counter electrode, which was a non-corroding steel mesh, and an RE, to monitor the potential of WE. The saturated

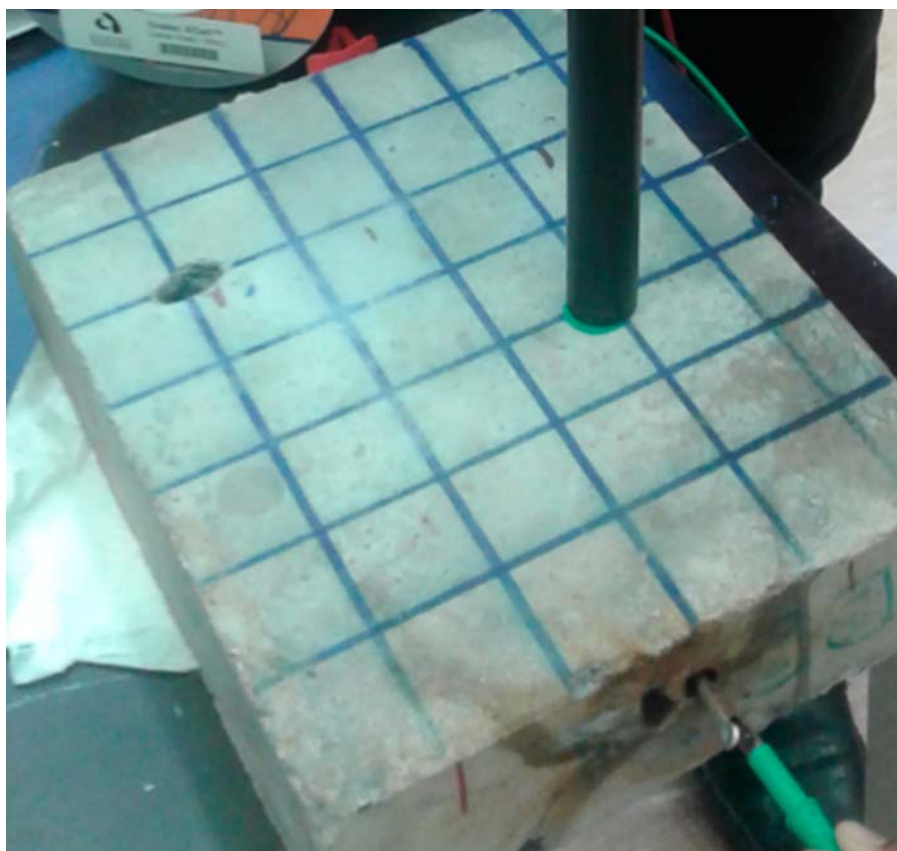


Plate 2.
Half-cell potential
measurements on
concrete blocks using
Cu/CuSO₄ as the
reference electrode

calomel electrode (SCE) was used for these experiments. The LPR technique measures the resistance to charge transfer of a metal; higher the polarization resistance, more corrosion resistant is the metal. In LPR a small polarization is applied on either sides of an open circuit potential (OCP) of steel rebar. The slope of this polarization curve gives the polarization resistance (R_p), as mentioned in Equation (4). In this study, ± 20 mV polarization was applied with a scan rate of 0.167 mV/sec on either sides of OCP of steel rebar and current response was recorded:

$$R_p = \Delta E / \Delta I. \quad (4)$$

The following equation was used to obtain the corrosion current density i_{corr} ($\mu\text{A}/\text{cm}^2$), where Stern–Geary constant B is divided by R_p (refer to Equation (5)). Although B depends on Tafel constants, its values are fixed to 26 and 52 mV for active and passive corrosion state, respectively (Andrade and Alonso, 2004):

$$i_{corr} = B / R_p. \quad (5)$$

2.3.5 Tafel Plot. Tafel and Stern (1905) proposed that the logarithm of current varies with electrode potential (i.e. $\log I \sim E$) in an electrochemical reaction. A polarization of ± 200 mV is applied to metal from corrosion potential (E_{corr}) and a logarithmic response of current, I , is recorded. The extrapolation of these curves yields the corrosion parameters like I_{corr} , anodic Tafel slope constant β_a , and cathodic Tafel slope constant β_c . From I_{corr} , the corrosion current density i_{corr} is calculated by $\Delta I/S$, where S is the polarized steel surface area. The i_{corr} has units of microamperes per centimeter square ($\mu\text{A}/\text{cm}^2$).

2.3.6 Electrochemical impedance spectroscopy. ECR and ECRC samples could not be polarized by LPR and Tafel plot techniques, as the epoxy is an insulator material that does not allow DC current to pass through. The EIS technique injects AC polarization at a selected range of frequency. With EIS spectra, the concrete resistivity, R_c , resistance to charge transfer of the rebar, R_{ct} , double layer capacitance, C_{dl} , epoxy coating resistance, R_{EP}/R_2 , and epoxy capacitance, C_p , are obtained. To evaluate the corrosion state of underlying steel in ECR and ECRC samples, 15 mV AC perturbation at a frequency range of 0.001– 10^6 Hz was applied, whereas for BBs, the frequency range was 0.01– 10^6 Hz. Higher frequency ranges give the characteristics of bulk concrete (electrolyte), whereas lower frequencies give information on steel rebar (electrode). Impedance of the corrosion system is presented by Nyquist plots.

2.3.7 Gravimetric weight loss. To measure the weight loss due to the corrosion, the steel rebar samples were retrieved from concrete blocks after the electrochemical tests. Five (5) small-sized (≈ 50 mm in length) pieces were cut from each mild steel BB (Figure 5), and weight loss per unit area was measured using an analytical balance with a precision of 0.00001 g. Steel pieces were cleaned using Clark's solution according to the ASTM G-I-90

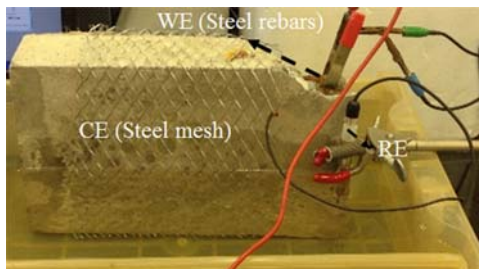


Figure 4.
Three-electrode setup
for Tafel plots

(1999) and then by the mechanical brushing. This cleaning process was repeated until the weight loss became constant. The weight of cut pieces after cleaning was compared to the nominal weight of a 16 mm diameter deformed steel rebar with similar length. The corrosion rate in mm/year was calculated by two methods: gravimetric analysis using Equation (6) and from the corrosion currents obtained from electrochemical techniques using Faraday's law (Equation (7)):

$$\text{Corrosion rate} \left(\frac{\text{mm}}{\text{year}} \right) = \frac{KW}{ATD} \tag{6}$$

$$\text{Corrosion rate} \left(\frac{\text{mm}}{\text{year}} \right) = \frac{3272I_{corr} EW}{dA}, \tag{7}$$

where K is a constant having value of 8.76×10^4 to obtain the corrosion rate in mm/year (ASTM G-I-90., 1999). T is exposure time in hours, A is the area in cm^2 , W is mass loss of steel bar in grams (g). Whereas I_{corr} is the corrosion current in μA , E.W is the equivalent weight of steel (55.87 g/mol) and D (d) is the density of reinforcing steel in g/cm^3 .

2.3.8 *Knife test for epoxy coating.* The adhesion of ECR and ECRCD was evaluated after retrieving from concrete blocks using the knife-peel test in accordance with the Ontario Ministry of Transportation (1993). It is recommended to apply two cuts of approximately 9 mm length each, making an X shape. Depending upon the condition of epoxy coating, an adhesion number from 1 to 5 is assigned, as presented in Figure 6 higher the number, more damaged is the epoxy coating and a larger area of epoxy will be peeled off. Further, the color of epoxy turns from dark green to brownish due to the deterioration by aggressive agents or by the presence of corrosion products underneath the epoxy.

Figure 5.
Cut pieces of bare bars, cleaning in Clark's solution with ultrasonic bath



Adhesion number	Description of tested area	Epoxy condition
1	Unable to insert blade tip under coating	
2	Total area of exposed steel <math>< 2 \text{ mm}^2</math>	
3	<math>2 <math>>="" <math><="" 4="" \text{="" \text{total="" area="" exposed="" math>="" math><="" mm}^2<="" of="" steel}<="" td=""> <td></td> </math>2>	
4	Total area of exposed steel >math>> 2 \text{ mm}^2</math>	
5	Blade tip slides easily under coating, levering action removes entire section (approximately <math>40 \text{="" coating<="" math>)="" mm}^2<="" td=""> <td></td> </math>40>	

Figure 6.
Adhesion number for epoxy coating

Source: Ontario Ministry of Transportation (1993)

3. Results and discussion

3.1 Concrete resistivity

Figure 7 presents the measured resistivity of a C40 concrete after two years of exposure under seawater. Column bars have an average resistivity from three blocks having similar reinforcement, whereas error bars show maximum and minimum values. An average resistivity over nine samples was 7,670 Ω-cm, with minimum and maximum of 5,024 Ω-cm (BB) and 12,362 Ω-cm (ECR), respectively. The resistivity of concrete samples reinforced with mild steel BB was lower than the one reinforced with ECR. This could be due to the cracking induced in concrete by heavy corrosion products. Table III presents the corrosion risk associated with concrete resistivity suggested by different researchers from open literature (Song and Saraswathy, 2007). Most concrete blocks had resistivity values at which the corrosion risk is high to very high. Given the lower resistivity and presence of moisture, the concretes under marine environment have higher diffusivity to ions like Fe²⁺, Cl⁻ and OH⁻, hence the risk of corrosion becomes higher in such conditions.

3.2 Chloride profile

Figure 8 presents the chloride ion concentration along the depth of concrete blocks. Generally, the concentration of chlorides decreases from a maximum value at the outer surface to a minimum value at the middle of the concrete member. The thickness of concrete blocks was 70 mm, whereas the clear cover was only 25 mm, and several (48 in total) wetting and drying cycles were applied for two years, hence the chloride profiles were observed to be quasi-constant till steel surface. Minimum chloride

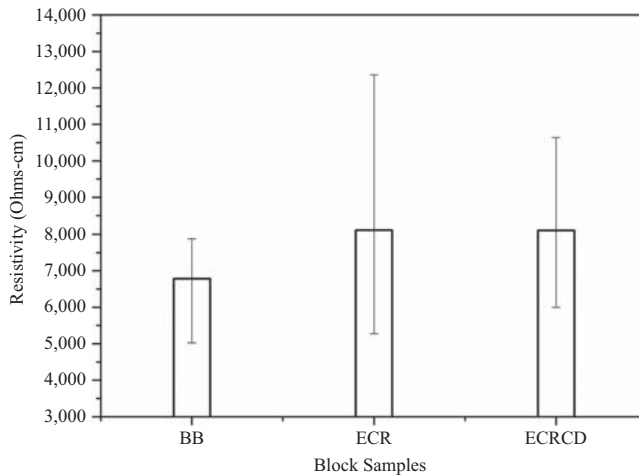


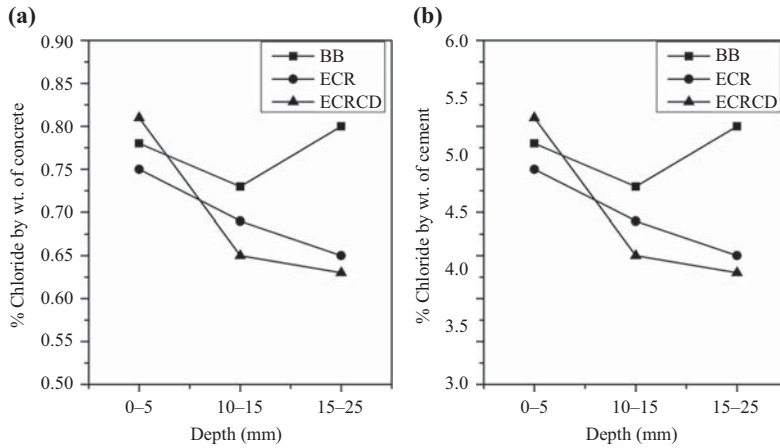
Figure 7. Resistivity values measured at concrete samples after two years of immersion in seawater

Resistivity (Ω-cm)	Corrosion risk
--------------------	----------------

> 20,000	Negligible
10,000–20,000	Low
5,000–10,000	High
< 5000	Very high

Source: Song and Saraswathy (2007)

Table III. Corrosion risk related to concrete resistivity expressed by different researchers



Notes: (a) % by wt. of concrete; (b) % by wt. of cement

Figure 8.
Chloride profile in
blocks samples

concentration near the steel surface was at least 0.63 percent by weight of concrete in all samples, whereas the maximum value was 0.80 percent. Figure 8(b) shows the % chloride contents against the weight of cement. The risk of corrosion of steel rebar increases with chloride ions concentration. According to (Broomfield, 2007) 0.4 percent of chloride by weight of cement is the threshold value for corrosion to be initiated. Some other researchers (Funahashi, 1990) suggested the Cl⁻ threshold of 0.17 percent by weight of cement; however, a threshold of 0.2 and 0.25 percent is also mentioned in other literature (Glass and Buenfeld, 1997). Table IV shows the risk of corrosion involved with chloride ions concentration with respect to the total mass of both concrete and cement, respectively (Broomfield, 2007). For a high risk of corrosion, chloride concentration is suggested as 0.14 percent by weight of concrete.

The chloride concentration after two years of immersion in seawater with 3.89 percent NaCl⁻ is 6 times higher than the threshold values for corrosion initiation mentioned in the literature. This shows that a normal concrete could absorb very large quantities of chlorides by diffusion process from the surrounding environment, especially at splash zone where wetting and drying cycles are encountered. The results of HCP, Tafel plot and weight loss measurements indicate severe corrosion of mild steel BB, whereas at this high concentration of chlorides ions, the ECR and ECRCD have not shown any corrosion initiation. Darwin *et al.* (2009) have studied the chloride threshold for ECR, galvanized rebar and mild steel rebar. It was observed that ECR could withstand about 4 times higher concentrations of chloride ions before corrosion initiation and damage to the epoxy coating. The reported threshold for ECR, galvanized steel and for mild steel was 4.32, 1.52 and 0.93 kg/m³, respectively, (Darwin *et al.*, 2009).

Table IV.
The risk of corrosion
with % chloride
concentration
by weight of
concrete and cement

% Chloride by weight of cement	% Chloride by weight of concrete	Risk level
< 0.2	< 0.03	Negligible
0.2-0.4	0.03-0.06	Low
0.4-1.0	0.06-0.14	Moderate
> 1.0	> 0.14	High

Source: Broomfield (2007)

3.3 Half-cell potential

Figure 9 shows the half-cell potential (HCP) contour mapping on the surface of BB-3, ECR-3 and ECRCD-3. The whole surface of the concrete block gave potential below -600 mV/CSE with a minimum HCP value of -732 mV/CSE. ASTM C876-09 (2015) standard suggests severe corrosion at BB (Table V). Corrosion products were visible at the surface of BB samples, especially at the side where reinforcement had a bent. The HCPs at ECR and ECRCD were observed to be in the range of -40 mV/CSE to -350 mV/CSE, as shown in Figure 9(b) and (c), respectively. These potentials are less electronegative compared to mild steel BB. This shows that ECR and ECRCD were in passive state and high chloride concentration was not able to damage or penetrate through the epoxy coating. According to ASTM C876-09 (2015), the probability of corrosion at these HCPs values is low (Table V).

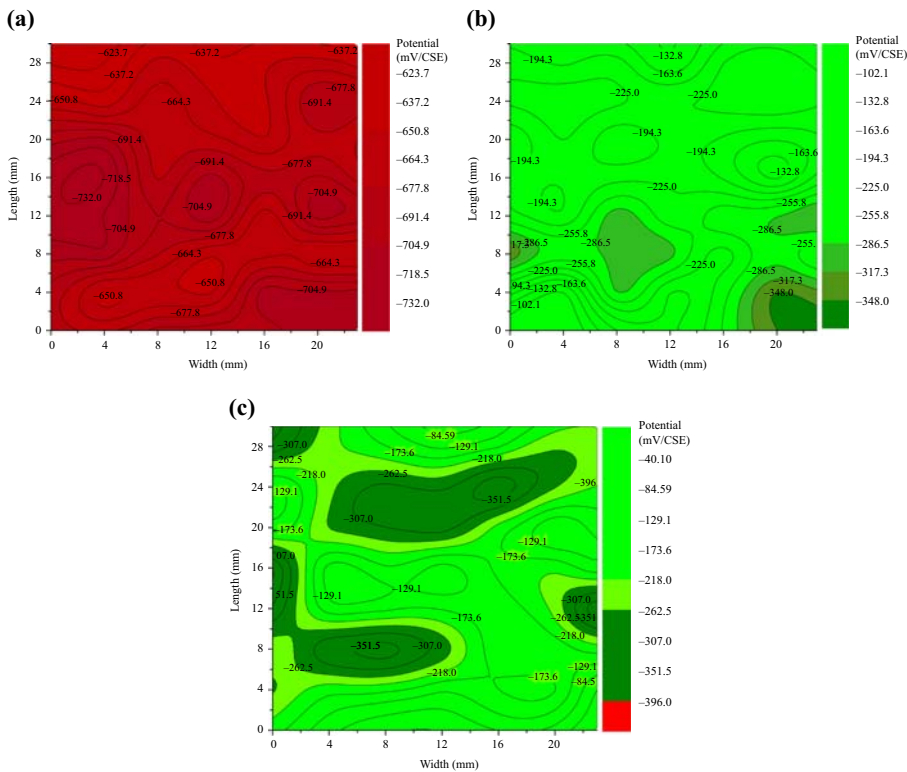


Figure 9. Half-cell potential measured

Notes: (a) BB-3; (b) ECR-3; (c) ECRCD-3

mV vs SCE	OPC values	mV vs CSE	Corrosion conditions
Less than -426		Less than -500	Severe corrosion
Less than -276		Less than -350	High (higher than 90% risk of corrosion)
-126 to -275		-200 to -350	Intermediate corrosion risk
Higher than -125		Higher than -200	Low (10% risk of corrosion)

Source: ASTM C876-09 (2015)

Table V. Half-cell potential values for corrosion conditions

The potential of ECRCD suggested that the small damages to epoxy were not able to initiate the corrosion at the steel surface. Keßler *et al.* (2016) suggested that the damages will only be harmful in the case where a macro-cell is formed between these damages and an uncoated rebar or other defected portion. Then these defects could act as a cathode and cause disbondment of epoxy near the damaged surface.

3.4 Linear Polarization resistance

Figure 10 shows the polarization curves for samples BB-2 and BB-3 obtained in LPR technique. LPR was not used for ECR and ECRD samples, as DC current could not pass through the epoxy coating. R_p values of 4.5 and 7.75 $k\Omega\text{ cm}^2$ were observed for BB-2 and BB-3, respectively. Passive steel shows an R_p value above 230 $k\Omega\text{ cm}^2$ (Vedalakshmi and Palaniswamy, 2010); below this value, the corrosion initiation is imminent. Hence, severe corrosion is associated with such lower polarization resistance.

3.5 Electrochemical impedance spectroscopy

Nyquist plots for BB, ECR and ECRCD from EIS scan are shown in Figure 11. Depending upon the configuration of the interfaces in RC, the response is compared to an equivalent circuit model to obtain the parameters like R_c , R_{ct} , resistance of the epoxy coating, R_2 (R_{EP}) and capacitance, C_p . Figure 12 shows the equivalent circuit model used to fit the experimental EIS curves. Three capacitive arcs, i.e., three-time constants, appear at different frequency ranges. Due to the heterogeneity of concrete and roughness of electrode surface, the interfaces do not act as pure capacitors; hence, the semi-circles are overlapping and depressed below the real axis in the Nyquist plot. For this reason, instead of using a pure capacitor in the circuit, a constant phase element (CPE), Q_i , is added that allows the best fitting of the curve (Figure 12). Capacitance from CPE was then calculated by Equation (8). The obtained parameters are shown in Table VI. The curves of BB are similar in behavior, at the lower frequencies, the impedance of electrode reactions is observed providing R_{ct} . The values of R_{ct} in case of BB-2 and BB-3 were 6.02 and 9.03 $k\Omega\text{ cm}^2$, respectively. The middle arc is due to oxide and concrete micro-structure at the steel surface. Some researchers attributed this middle arc to the lime precipitation at the steel surface with an oxide layer (Dhouibi-Hachani *et al.*, 1996; Lay *et al.*, 1985). In carbonated concrete where lime is consumed in the carbonation process, this arc does not appear. In

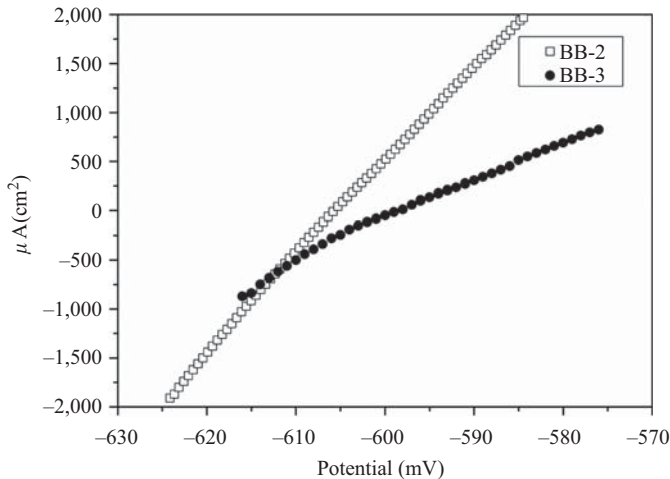


Figure 10. R_p of mild steel bare bar samples, BB-2 and BB-3

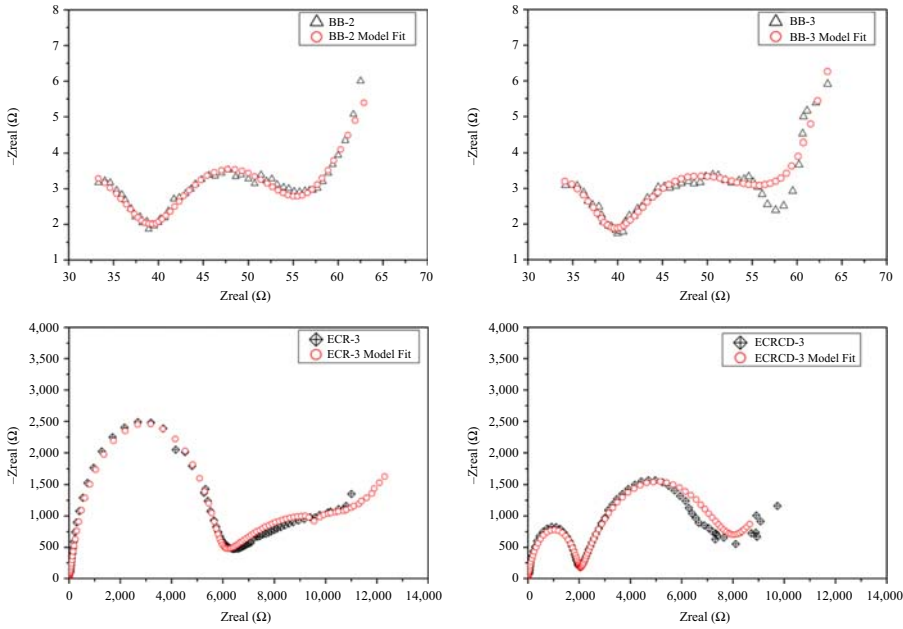


Figure 11. Nyquist plot for a mild steel bare bar, ECR and ECRCD

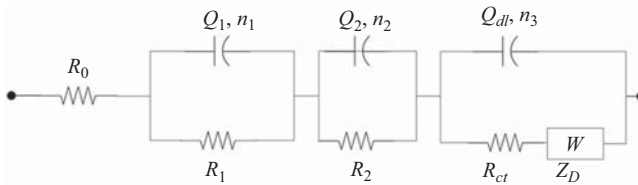


Figure 12. Equivalent circuit model for EIS spectra

	R_c Ω	R_2/R_{EP} Ω	C_2/C_p $\mu F.cm^{-2}$	R_{ct} $k\Omega.cm^2$
BB-2	36	20	9.24E-05	6.02
BB-3	40	12	4.66E-04	9.03
ECR-3	38	5,926	2.73E-05	1,673
ECRCD-3	28	2005	2.54E-05	1,675

Table VI. Electrochemical impedance parameters

the case of ECR, the middle arc provides the characteristics of the epoxy layer. ECR and ECRCD show different behaviors in this region. The resistance of the epoxy coating was 1,784 and 604 $k\Omega cm^2$ in ECR and ECRCD, respectively. Lower resistance in ECRCD shows that the EIS technique was able to detect the defects in epoxy, and hence can be a useful tool in accessing the epoxy condition and corrosion of underlying steel. At this frequency range, the block samples with BBs showed resistance of 6 and 24 $k\Omega cm^2$, that is, the resistance offered by oxide and lime layer precipitated at steel surface. The R_{ct} values of ECR and ECRCD samples were 1,673 and 1,675 $k\Omega cm^2$, respectively, which is a very high resistance to charge transfer, showing that the underlying steels are in a passive corrosion state. An inclined upward line at the right of Nyquist plot shows the Warburg

diffusion, W , which is the diffusion of ions through the interfaces formed between concrete and passive layer at steel surface in BB and concrete and epoxy coating in ECR:

$$C = Q^{1/n} R^{(1-n)/n} \tag{8}$$

3.6 Tafel plots

Figure 13 shows the Tafel plot of BB-2 and BB-3 obtained by applying polarization of ± 200 mV. Extrapolation of these curves gives the corrosion current (I_{corr}) and the anodic and cathodic Tafel slopes, β_a and β_c , respectively. Results are presented in Table VII. Corrosion current densities were observed to be 1.24 and $0.40 \mu\text{A}/\text{cm}^2$ on BB-2 and BB-3, respectively. The β_a was 420 millivolts per decade (mV/dec) and 440 mV/dec, whereas β_c was 438 and 415 mV/dec for BB-2 and BB-3, respectively. The slope of the linear portion of the Tafel plot indicates the rate of corrosion reaction: steeper the slope, higher is the rate of corresponding half-cell reaction. Table VIII lists the corrosion severity with respect to the measured corrosion current density. The corrosion current densities were in the range of moderate to high or very high. These corrosion parameters form Butler–Volmer equation, which alongside Ohm’s law are used to model the corrosion phenomenon in RC

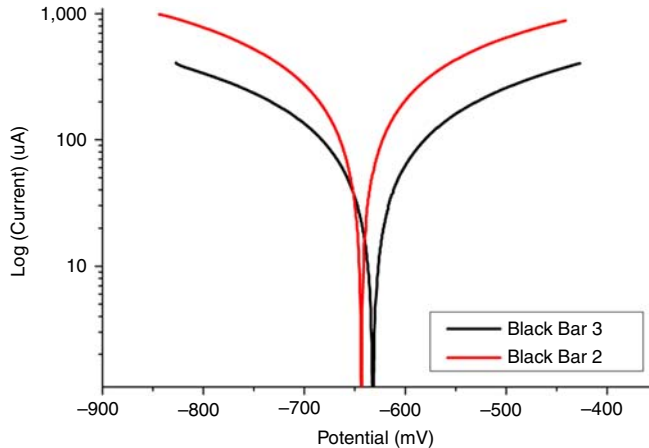


Figure 13. Tafel plots (polarization curves)

Sample	Corrosion currents		Tafel slopes	
	I_{corr} μA	i_{corr} $\mu\text{A}/\text{cm}^2$	β_a mV/dec	β_c mV/dec
BB-2	360	1.24	420	438
BB-3	120	0.4	440	415

Table VII. Corrosion parameters from Tafel plots

Corrosion current (I_{corr})	Conditions of rebar
$< 0.1 \mu\text{A}/\text{cm}^2$	Passive condition
$0.1\text{--}0.5 \mu\text{A}/\text{cm}^2$	Low-to-moderate corrosion
$0.5\text{--}1.0 \mu\text{A}/\text{cm}^2$	Moderate-to-high corrosion
$> 1.0 \mu\text{A}/\text{cm}^2$	High corrosion rate

Table VIII. Corrosion current density vs condition of the rebar

Source: Song and Saraswathy (2007)

(Gulikers and Raupach, 2006; Sohail *et al.*, 2015). The reported parameters will be useful for scientists and engineers to select suitable input parameters to simulate the corrosion in chloride-contaminated concrete.

3.7 Gravimetric weight loss

Figure 14 compares the weight at retrieval and after cleaning of cut steel pieces against their nominal weights. To normalize, the weight loss per unit area (g/cm^2) was calculated. The weight losses of 0.254 and $0.207 \text{ g}/\text{cm}^2$ on BB-2 and BB-3, respectively, were observed. A higher weight loss on BB-2 than BB-3 is in accordance with the results of LPR, EIS and Tafel plots in which the corrosion current density was also higher in BB-2 than BB-3.

Figure 15 presents the comparison of corrosion rate in mm/year on cut steel pieces through gravimetric method against the one calculated from corrosion current density measured by electrochemical techniques. On the steel pieces from BB-2, the average, maximum and minimum corrosion rates through gravimetric method were 0.06, 0.153 and $0.00327 \text{ mm}/\text{year}$, respectively (Figure 15). For BB-3, these values were 0.0565, 0.113

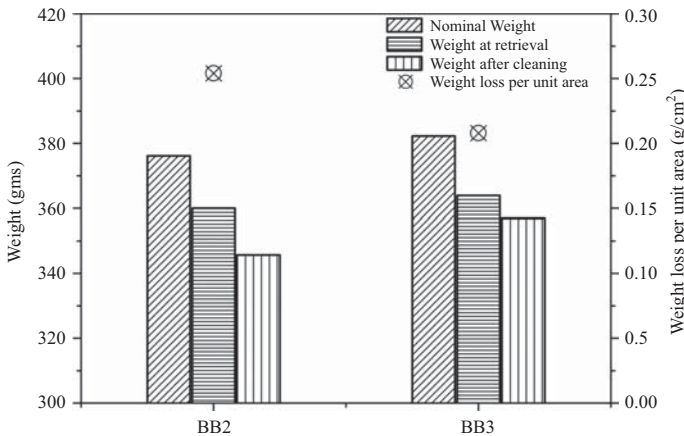


Figure 14. Weight loss of cut pieces of steel bars from BB-2 and BB-3

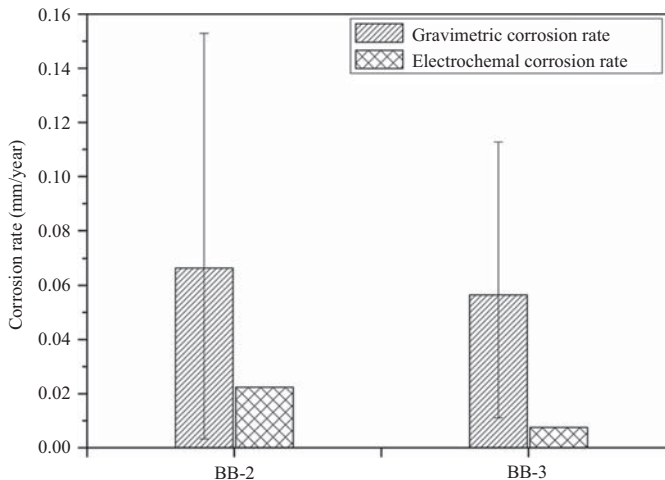


Figure 15. Corrosion rate through gravimetric weight loss and corrosion current density at BB-2 and BB-3

and 0.0111 mm/year, respectively (Figure 15). The corrosion rates from electrochemical method were 0.0224 and 0.00747 mm/year for rebar from BB-2 and BB-3, respectively.

Higher corrosion rates calculated through gravimetric weight loss, than from Faraday's law, are attributed to two factors, first, in the electrochemical methods, the uniform polarization of the whole surface of steel embedded in concrete is not always achievable. This results in an underestimation of corrosion currents. Second, since the chloride attack causes the localized (pitting) corrosion at steel surface, for the growth and survival of these pits, availability of large cathodic surface area and availability of OH^- to react with Fe^{2+} are compulsory (Angst *et al.*, 2012). Otherwise, the bottom of pits will be re-passivated. These pitting surfaces, when polarized with applied voltage in electrochemical techniques, will respond in less current and will hence result in an underestimation of actual corrosion activities.

3.8 Knife-peel test and visual inspection

An adhesion number of 1 was observed in knife-peel tests; the epoxy coating was hard to cut through by the knife blade. Epoxy coating of ECR and ECRCD was strongly intact and no change in coating color was observed after two years of immersion. There was no evidence of steel corrosion under the epoxy coating. Plate 3 shows the corrosion conditions of ECR and BB after retrieval. Mild steel BB suffered severe corrosion and the rust products migrated into the adjacent concrete. Further, the U bent portions showed severe corrosion and the rust products were visible at the outer surface of concrete blocks, whereas the ECR and ECRCD were not affected by chlorides and moisture, the epoxy was in shining green color, no disbondment at the bent portion, and no corrosion of underlying steel was observed.

4. Conclusions

The corrosion performance of mild steel BB and ECR was evaluated by embedding them in concrete blocks samples that were conditioned under seawater for two years. The wetting and drying cycles were applied to accelerate the chloride diffusivity. The electrochemical tests, gravimetric analysis, and adhesion test were performed to assess the corrosion performance of both types of rebars after two years of exposure under accelerating aging conditions. Following are the main conclusions of the study:

- (1) ECR could withstand high chloride ion concentration at which the mild steel bare bar will severely corrode. After two years of immersion in seawater, the chloride concentration in a C40 concrete was observed to be between 0.63 and 0.80 percent by



Plate 3.
Visual inspection of corrosion conditions of BB, ECR and ECRCD in concrete blocks and after retrieval

- weight of concrete, which is six times higher than the established threshold for corrosion initiation in case of mild steel. No breakage to epoxy and no corrosion to underlying steel bar were observed.
- (2) Concrete resistivity, which is an indicator of the ease with which corrosion activities can take place on the steel–concrete interface, suggested a very high corrosion risk in concrete blocks after two years of immersion in seawater (≈ 3.89 percent NaCl^-).
 - (3) Further, HCP of mild steel rebar was below -600 mV/CSE, which ensures higher corrosion activities, whereas for ECR and ECRCD, it was around -100 mV/CSE— 350 mV/CSE, which suggests passivity or no corrosion.
 - (4) Polarization resistance measured by LPR was 4.5 and 7.75 $\text{k}\Omega\text{ cm}^2$, and by EIS technique, it was 6.02 and 9.03 $\text{k}\Omega\text{ cm}^2$ on mild steel BB (BB-2 and BB-3, respectively). These values indicate higher corrosion rates. The ECR and ECRCD showed very high charge transfer resistance of $1,672$ and $1,675$ $\text{k}\Omega\text{ cm}^2$ in EIS spectra, respectively. Hence, no corrosion activity was observed at ECRs.
 - (5) Tafel plot results showed the corrosion current densities of 1.24 and 0.40 $\mu\text{A}/\text{cm}^2$ on BB-2 and BB-3, respectively, suggesting very higher corrosion rates at mild steel rebar. β_a was 420 millivolts per decade (mV/dec) and 440 mV/dec for BB-2 and BB-3, respectively, whereas β_c was 438 and 415 mV/dec for BB-2 and BB-3, respectively. These values could be used as input parameters in the numerical modeling of corrosion in concrete.
 - (6) The corrosion rates measured through gravimetric weight loss were observed to be higher than those calculated by corrosion current density in the Tafel plot. This was due to non-uniform polarization of steel surface and re-passivation of pits, which results in an underestimation of corrosion activities.
 - (7) The controlled damaged ECR also showed no corrosion activities, which suggests that the small defects have no effect on ECR performance, especially when there is no macro-cell connection with uncoated rebar. Hence, while placing the steel reinforcements, the plastic connecting wires should be used instead of steel wires to avoid any short circuit between defects on ECR and uncoated rebar.

References

- AASHTO TP 95 (2011), *Standard Method of Test for Surface Resistivity Indication of Concrete's Ability to Resist Chloride Ion Penetration*, American Association of State Highway and Transportation Officials, Washington, DC, available at: <http://standards.globalspec.com/std/9863485/aashto-tp-95> (accessed December 22, 2017).
- Ahmad, S. (2009), "Techniques for inducing accelerated corrosion of steel in concrete", *The Arabian Journal for Science and Engineering*, Vol. 34 No. 2C, pp. 95-104.
- Al-Khaiat, H., Jones, B. and Haque, M.N. (2007), "Designing durable concrete structures in The Arabian Gulf: a draft code", *32nd Conference on Our World in Concrete & Structures, Singapore, August 28-29*.
- Al-Samarai, M. (2015), "Durability of concrete in the Arabian Gulf", *Journal of Materials Science and Engineering A*, Vol. 5 Nos 11-12, pp. 398-408.
- Andrade, C. and Alonso, C. (2004), "Test methods for on-site corrosion rate measurement of steel reinforcement in concrete by means of the polarization resistance method", *Materials and Structures*, Vol. 37 No. 9, pp. 623-643.
- Angst, U., Elsener, B., Jamali, A. and Adey, B. (2012), "Concrete cover cracking owing to reinforcement corrosion – theoretical considerations and practical experience", *Materials and Corrosion*, Vol. 63 No. 12, pp. 1069-1077.

- ASTM A775/A775M – 17 (2017), “Standard Specification for epoxy-coated prefabricated steel reinforcing bars 1”, ASTM International, West Conshohocken, PA, pp. 1–19.
- ASTM C876-09 (2015), “Standard test method for half-cell potentials of uncoated reinforcing steel in concrete”, ASTM, 91(Reapproved), pp. 1-6, doi: 10.1520/C0876-09.2.
- ASTM G-I-90 (1999), “Practice for preparing, cleaning, and evaluating corrosion test specimens”, available at: www.astm.org/DATABASE.CART/HISTORICAL/G1-90R99E1.htm (accessed February 21, 2013).
- Bazant, Z.P. (1983), “Journal of structural engineering”, *ASCE J Struct Div, American Society of Civil Engineers*, Vol. 105 No. 6, pp. 1137-1153.
- Broomfield, J.P. (2007), *Corrosion of Steel in Concrete: Understanding, Investigation and Repair*, Taylor & Francis, London.
- BS 1881: Part-124 (1998), “British standard testing concrete part 124. methods for analysis of hardened concrete”, available at: www.c-s-h.ir/wp-content/uploads/2015/10/BS-1881-Part-124-88.pdf (accessed March 19, 2017).
- Darwin, D., Browning, J., O’Reilly, M., Xing, L. and Ji, J. (2009), “Critical chloride corrosion threshold of galvanized reinforcing bars”, *ACI Materials Journal*, Vol. 106 No. 2, pp. 176-183.
- Dhouibi-Hachani, L., Triki, E., Grandet, J. and Raharinaivo, A. (1996), “Comparing the steel-concrete interface state and its electrochemical impedance”, *Cement and Concrete Research*, Vol. 26 No. 2, pp. 253-266.
- Djerbi, A., Bonnet, S., Khelidj, A. and Baroghel-bouny, V. (2008), “Influence of traversing crack on chloride diffusion into concrete”, *Cement and Concrete Research*, Vol. 38 No. 6, pp. 877-883.
- Duffó, G.S., Reinoso, M., Ramos, C.P. and Farina, S.B. (2012), “Characterization of steel rebars embedded in a 70-year old concrete structure”, *Cement and Concrete Research*, Vol. 42 No. 1, pp. 111-117.
- Dunn, R.C., Ross, R.A. and Davis, G.D. (2010), “Corrosion monitoring of steel reinforced concrete structures using embedded instrumentation”, *NACE Corrosion Conference & Expo*, pp. 1-10.
- Elsener, B., Andrade, C., Gulikers, J., Polder, R. and Raupach, M. (2003), “Hall-cell potential measurements – potential mapping on reinforced concrete structures”, *Materials and Structures*, Vol. 36 No. 7, pp. 461-471.
- EN 206-1 (2000), *EN 206-1. Performance-Based Specifications and Control of Concrete Durability, Concrete, Part 1, Specification, Performance, Production and Conformity*, Institution, British Standards, London.
- Erdođdu, Œ., Bremner, T. and Kondratova, I. (2001), “Accelerated testing of plain and epoxy-coated reinforcement in simulated seawater and chloride solutions”, *Cement and Concrete Research*, Vol. 31 No. 6, pp. 861-867.
- Funahashi, M. (1990), “Predicting corrosion-free service life of a concrete structure in a chloride environment”, *ACI Materials Journal*, Vol. 87 No. 6, pp. 581-587.
- Glass, G.K. and Buenfeld, N.R. (1997), “The presentation of the chloride threshold level for corrosion of steel in concrete”, *Corrosion Science*, Vol. 39 No. 5, pp. 1001-1013.
- Gulikers, J. and Raupach, M. (2006), “Modelling of reinforcement corrosion in concrete-preface”, *Materials and Corrosion*, Vol. 57 No. 8, pp. 603-604.
- Keßler, S., Angst, U., Zintel, M., Elsener, B. and Gehlen, C. (2016), “Epoxy-coated reinforcement in concrete structures: Results of a Swiss pilot project after 24 years of field exposure”, *Materials and Corrosion*, Vol. 67 No. 6, pp. 631-638.
- Khaled, K.Z., Vaca-Cortes, E., Jisra, J., Wheat, H. and Carrasquillo, R.L. (1998), *Corrosion Performance of Epoxy-coated Reinforcement-Beam Tests*, Center for Transportation Research Bureau of Engineering Research The University of Texas at Austin, TX.
- Lay, P., Lawrence, P.F., Wilkins, N.J.M. and Williams, D.E. (1985), “An a.c. impedance study of steel in concrete”, *Journal of Applied Electrochemistry*, Vol. 15 No. 5, pp. 755-766.

- Liu, Y. and Weyers, R.E. (1998), "Modeling the time-to-corrosion cracking in chloride-contaminated reinforced concrete structures", *ACI Materials Journal*, Vol. 95 No. 6, pp. 675-681.
- McDonald, D. (2009), "Epoxy-coated reinforcing steel bars in Northern America", available at: www.researchgate.net/publication/257121418_EPOXY-COATED_REINFORCING_STEEL_BARS_IN_NORTHERN_AMERICA (accessed April 7, 2018).
- Manning, D.G. (1996), "Corrosion performance of epoxy-coated reinforcing steel: North American experience", *Construction and Building Materials*, Vol. 10 No. 5, pp. 349-365.
- Maslehuddin, M.O.S.B. and Al-Amoudi, M.K.R.M.R.A. (2007), "Concrete deterioration in the Arabian Gulf – developments in preventive techniques", *International Conference on Advances in Cement Based Materials and Applications to Civil Infrastructure (ACBM-ACI)*, Lahore, December 12-14.
- Nagi, M. and Whiting, D. (2004), "Resistivity of concrete: state of the art", NACE International, available at: www.onepetro.org/conference-paper/NACE-04326 (accessed March 22, 2017).
- Nasser, A. (2010), "La corrosion des aciers dans le béton à l'état passif et par carbonatation : prise en compte des courants galvaniques et des défauts d'interface acier-béton", available at: <http://thesesups.ups-tlse.fr/1091/> (accessed February 20, 2013).
- Ontario Ministry of Transportation (1993), *Ontario Provincial Standards for Roads and Public Works*, Kingston.
- Pakkala, T.A., Kōliö, A., Lahdensivu, J. and Pentti, M. (2019), "Predicted corrosion rate on outdoor exposed concrete structures", *International Journal of Building Pathology and Adaptation*, doi: 10.1108/IJBPA-11-2018-0086.
- Polder, R.B. and Hug, A. (2000), "Penetration of chloride from de-icing salt into concrete from a 30 year old bridge", *Heron*, Vol. 45 No. 2, pp. 109-124.
- Poon, C.S. and Baldwin, G.R. (1990), "Influence of weather on the corrosion of steel reinforcement in Hong Kong", *Structural Survey*, Vol. 8 No. 2, pp. 169-176, doi: 10.1108/EUM000000003221.
- Pyc, W. (1998), "Field performance of epoxy-coated reinforcing steel in Virginia bridge decks", available at: <https://vtechworks.lib.vt.edu/handle/10919/29399> (accessed April 2, 2018).
- Qatalum (2006), "Environmental impact assessment", Doha, available at: www.qatalum.com/AboutUs/Sustainability/pages/eia-report.aspx (accessed December 13, 2017).
- Rasheeduzzafar, D.F.H., Bader, M.A. and Khan, M.M. (1992), "Performance of corrosion-resisting steels in chloride-bearing concrete", *ACI Materials Journal*, Vol. 89 No. 5, pp. 439-448.
- Sohail, M.G. (2013), "Corrosion of steel in concrete: development of an accelerated test by carbonation and galvanic coupling", available at: <http://thesesups.ups-tlse.fr/1938/> (accessed July 2, 2014).
- Sohail, M.G., Kahraman, R., Ozerkan, N.G. and Alnuaimi, N.A. (2018), "Reinforced concrete degradation in the harsh climates of the Arabian Gulf: field study on 30-to-50-year-old structures", *Journal of Performance of Constructed Facilities*, Vol. 32 No. 5, pp. 1-12.
- Sohail, M.G., Laurens, S., Deby, F. and Balayssac, J.P. (2015), "Significance of macrocell corrosion of reinforcing steel in partially carbonated concrete: numerical and experimental investigation", *Materials and Structures/Materiaux et Constructions*, Vol. 48 Nos 1-2, pp. 217-233.
- Song, H.W. and Saraswathy, V. (2007), "Corrosion monitoring of reinforced concrete structures – a review", *International Journal of Electrochem Science*, Vol. 2, June, pp. 1-28.
- Tafel, J. and Stern, H. (1905), "Ueber Diaminobornsteinsäureäthylester", *Berichte der deutschen chemischen Gesellschaft*, Vol. 38 No. 2, pp. 1589-1592.
- Tasker, J.S. (1985), "'Concrete disease – diagnosis and cure', structural survey", *MCB UP Ltd*, Vol. 3 No. 1, pp. 6-11, doi: 10.1108/eb006200.
- Tuutti, K. (1982), *Corrosion of Steel in Concrete*, Swedish Cement and Concrete Research Institute, Stockholm, available at: <https://lucris.lub.lu.se/ws/files/4709458/3173290.pdf>

Vedalakshmi, R. and Palaniswamy, N. (2010), "Analysis of the electrochemical phenomenon at the rebar-concrete interface using the electrochemical impedance spectroscopic technique", *Magazine of Concrete Research*, Vol. 62 No. 3, pp. 177-189.

Virmani, Y.P., CLEAR, K.C. and Pasko, T.J. Jr (1983), *Time to Corrosion of Reinforcing Steel in Concrete Slabs, Vol.5: Calcium Nitrite Admixture and Epoxy-Coated Reinforcing Bars as Corrosion Protection Systems*, National Technical Information Service, Springfield, available at: <https://trid.trb.org/view.aspx?id=199231> (accessed March 19, 2017).

Yingshu, Y., Yongsheng, Ji and Shah, S.P. (2007), "Comparison of two accelerated corrosion techniques for concrete structures", *ACI Structural Journal*, Vol. 104 No. 3, pp. 344-347.

Further reading

Kehr, A. (2005), "Fusion-bonded epoxy coatings: a technology for rebar corrosion prevention".

Corresponding author

Ramazan Kahraman can be contacted at: ramazank@qu.edu.qa